(Preprint) AAS 24-045

FLIGHT PERFORMANCE COMPARISON OF BANK-ANGLE STEERING AND ALPHA-BETA STEERING FOR MARS ENTRY SYSTEMS

Daniel L. Engel[*], Zachary R. Putnam[†], Robyn M. Woollands[‡], and Soumyo Dutta[§]

Alpha-beta steering is an alternative hypersonic steering scheme to state-of-the-art bank-angle steering systems for guided Mars entry vehicles. This study uses optimal control to generate steering commands for a large robotic Mars entry vehicle using either a bank-angle or alpha-beta steering system to provide a more equal comparison of these two hypersonic steering options, not dependent on guidance design or the inclusion of conventional bank reversals. Objectives maximizing terminal altitude or minimizing control effort, while also reaching a desired target point are considered for both steering options in nominal and dispersed cases. Results indicate both steering options have similar performance, although alpha-beta steering is shown to have improved targeting performance, particularly for the latitude/crossrange. Alpha-beta steering is also able to reach higher terminal altitudes by about 0.25 km, relative to the vehicle using bank-angle steering. The difference in altitude maximization capability grows as the allowable vehicle rates decrease.

INTRODUCTION

The entry systems for the recent Mars 2020[1] and Mars Science Laboratory[2] (MSL) missions have utilized bank-angle steering for hypersonic trajectory control. Bank-angle steering is the current state-of-the-art for hypersonic trajectory control and has also been used at Earth for the Apollo Command Module,[3] Space Shuttle,[4] and Orion spacecraft.[5] While successful so far, control over the longitudinal and lateral motion is highly coupled for bank-angle steering systems.[6] Most existing guidance algorithms for bank-angle steering systems have controlled the longitudinal motion by choosing the bank angle magnitude either through analytical expressions (e.g. Apollo final phase guidance algorithm[2]) or by using one-dimensional root solving with numerical integration (numerical predictor-corrector guidance[7,8]). The lateral motion of the entry vehicle is then addressed using open-loop bank reversals, in which the sign of the bank angle is periodically switched. Bank reversals can have a negative impact on entry performance by providing a perturbation in the trajectory as well as a deviation from desired steering commands.[6] Vehicles using bank-angle steering also have other systems disadvantages including significant ballast mass to create the center-of-gravity

[*]PhD Candidate, Department of Aerospace Engineering, University of Illinois at Urbana-Champaign, 104 S. Wright St., Urbana, IL 61801

[†]Adjunct Assistant Professor, Department of Aerospace Engineering, University of Illinois at Urbana-Champaign, 104 S. Wright St., Urbana, IL 61801

[‡]Assistant Professor, Department of Aerospace Engineering, University of Illinois at Urbana-Champaign, 104 S. Wright St., Urbana, IL 61801

[§]Aerospace Engineer, Atmospheric Flight and Entry Systems Branch, 1 N. Dryden St., M/S 489

offset for steering[9] and the use of reaction control system (RCS) thrusters, which may interfere with the hypersonic wake behind the entry vehicle.[10–13]

A proposed alternative to bank-angle steering is alpha-beta (α-β) steering which involves independent modulation of the angle of attack (α) and the sideslip angle (β). A vehicle using α-β steering can use these aerodynamic angles to modulate the magnitudes of the aerodynamic lift, side force, and drag (bank-angle steering on blunt-body vehicles can only modulate the direction of the lift) and has less coupling over the longitudinal and lateral motion, relative to a vehicle using bank-angle steering.[6] Sometimes referred to as direct force control (DFC), α-β has been assessed in mission concepts for entry, aerocapture, and aerogravity assist at several planetary destinations including Venus,[14] Earth,[15] Mars,[16] Titan,[17] and Neptune.[17] Several actuation concepts for α-β steering have been considered, including aerodynamic flaps,[18] center-of-gravity movement systems,[19] and a morphing vehicle structure.[6] α-β steering may have systems advantages over vehicles using bank-angle steering, including the elimination of large amounts of ballast mass and RCS, potentially enabling a larger payload or a lower cost.[9] There are a limited number of existing studies which have compared bank-angle steering and α-β steering. Some of these have been applied for aerocapture,[17] indicating α-β steering may be more robust to atmospheric dispersions, relative to bank-angle steering.[20] Two other studies have compared entry performance of bank-angle steering and α-β for entry targeting. Studies for the Pterodactyl vehicle concept considered a deployable entry vehicle with flaps at Earth using either α-β steering or a yaw-to-bank bank-angle steering system. Targeting of a parachute deploy condition indicated both steering options had similar performance.[15,21] Another study of entry performance of a human-scale Mars entry vehicle found α-β steering may provide increased landing accuracy, a lower propellant usage for powered-descent (perhaps due to less propellant needed to fly out errors as a result of improved targeting), and a lower total angle of attack usage, relative to an alternative bank-angle steering system.[22]

All of these previous comparisons, however, have relied on state-of-the-art predictor-corrector guidance schemes. While these guidance algorithms provide effective targeting, the relative performance when comparing α-β and bank-angle steering is dependent on the design and tuning of the individual guidance schemes. For example, there are various choices in the structure of the guidance and tuning parameters. Furthermore, there are other factors, such as the use of open-loop bank reversals with bank-angle steering systems; the use of these bank reversals is choice, and they have the potential to reduce the relative performance of a vehicle using bank-angle steering. These choices potentially result in an unfair comparison of the two hypersonic steering schemes, potentially changing the comparison from between two steering systems, to a comparison of two guidance designs. More sophisticated guidance schemes can utilize optimal control for steering command generation. Optimal control does not require a user-specified structure of the guidance profile, does not utilize open-loop control reversals, and has few tuning parameters, resulting in a more equal comparison of different steering options. Optimal control can provide multi-dimensional solutions considering a time-varying command profile, as opposed to one-dimensional line searches and constant commands used with conventional predictor-corrector entry guidance. Optimal control for on-board steering command generation has been considered for bank-angle steering in several studies using direct-based optimal control solvers,[23,24] and recent studies have also used convex optimization with an approximation to the entry dynamics for both entry[25,26] and aerocapture.[27] None of these studies, however, have considered α-β steering, nor has any comparison been made between α-β steering and bank-angle steering using sophisticated steering commands from optimal control. In this study, a commercial optimal control solver is used to provide steering commands in order to

compare flight performance of bank-angle steering and α-β steering for several different trajectory objectives during a Mars entry.

METHODOLOGY

Models and Equations of Motion

Three-degree-of-freedom (3DOF) trajectory analysis is used to analyze the motion of Mars entry vehicles using either bank-angle steering or α-β steering. The equations of motion[7] below describe the motion of an entry vehicle over an oblate, rotating, Mars and are solved using a fourth order Runge-Kutta method with a constant time step of 0.1 s. These equations of motion are representative of the "truth" dynamics in numerical simulations.

$$\dot{r} = V \sin\gamma \tag{1}$$

$$\dot{\theta} = \frac{V \cos\gamma \sin\psi}{r \cos\phi} \tag{2}$$

$$\dot{\phi} = \frac{V \cos\gamma \cos\psi}{r} \tag{3}$$

$$\dot{V} = -\frac{D}{m} - g_r \sin\gamma - g_\phi \cos\gamma \cos\psi + \Omega^2 r \cos\phi(\sin\gamma \cos\phi - \cos\gamma \sin\phi \cos\psi) \tag{4}$$

$$\begin{aligned}\dot{\gamma} = \frac{1}{V}\Bigg[\frac{L\cos\sigma}{m} + (V^2/r - g_r)\cos\gamma + g_\phi \sin\gamma \cos\psi + 2\Omega V \cos\phi \sin\psi \\ + \Omega^2 r \cos\phi(\cos\gamma \cos\phi + \sin\gamma \cos\psi \sin\phi)\Bigg]\end{aligned} \tag{5}$$

$$\begin{aligned}\dot{\psi} = \frac{1}{V}\Bigg[\frac{Y + L\sin\sigma}{m\cos\gamma} + \frac{V^2}{r}\cos\gamma \sin\psi \tan\phi + g_\phi \frac{\sin\psi}{\cos\gamma} \\ - 2\Omega V(\tan\gamma \cos\psi \cos\phi - \sin\phi) + \frac{\Omega^2 r}{\cos\gamma}\sin\psi \sin\phi \cos\phi\Bigg]\end{aligned} \tag{6}$$

In these equations of motion, r is the radial distance of the entry vehicle from the center of mars, θ is the longitude, ϕ is the latitude, V is the Mars-relative velocity, γ is the Mars-relative flight-path angle, and ψ is the Mars-relative azimuth angle. Ω is the rotation rate of Mars, m is the vehicle mass, σ is the bank angle, and g_r and g_ϕ are the components of the acceleration due to gravity, including J_2 effects:[7]

$$g_r = \frac{\mu}{r^2}\left[1 + J_2\left(\frac{R_m}{r}\right)^2(1.5 - 4.5\sin^2\phi)\right] \tag{7}$$

$$g_\phi = \frac{\mu}{r^2}\left[J_2\left(\frac{R_m}{r}\right)^2(3\sin\phi\cos\phi)\right] \tag{8}$$

Here, μ is the gravitational parameter, and R_m is the equatorial radius of Mars. D, L, and Y are the aerodynamic drag, lift, and side forces given by:

$$D = q_\infty s_{ref} C_D \tag{9}$$

$$L = q_\infty s_{ref} C_L \tag{10}$$

$$Y = q_\infty s_{ref} C_Y \tag{11}$$

The aerodynamic coefficients C_D, C_L, and C_Y are calculated using the MSL aerodynamics database,[28] and the density used to calculate q_∞ is determined using the Mars Global Reference Atmospheric Model (GRAM).[29] For bank-angle steering, a positive bank angle is defined as a bank to the right; for α-β steering a positive angle of attack coincides with pitch-up and a positive sideslip angle coincides with yawing to the left. The aerodynamic angles and forces on a blunt-body entry vehicle are shown in Figure 1 for both bank-angle steering and α-β steering. The 70 deg sphere-cone blunt-body entry vehicle under consideration is assumed to be a heavy entry vehicle for high-mass robotic payloads as a precursor to human missions, similar to current designs of the entry vehicle for the Mars Sample Retrieval Lander.[30] Vehicle parameters, including the mass, aerodynamic reference area, maximum allowable angle of attack α_{max}, minimum allowable angle of attack $-\alpha_{max}$, maximum allowable sideslip angle β_{max}, minimum allowable sideslip angle $-\beta_{max}$, and the constant angle of attack on the bank-angle steering system α_{bank} are provided in Table 1. Such characteristics result in a hypersonic ballistic coefficient of about 203.5 kg/m^2 at zero angle of attack.

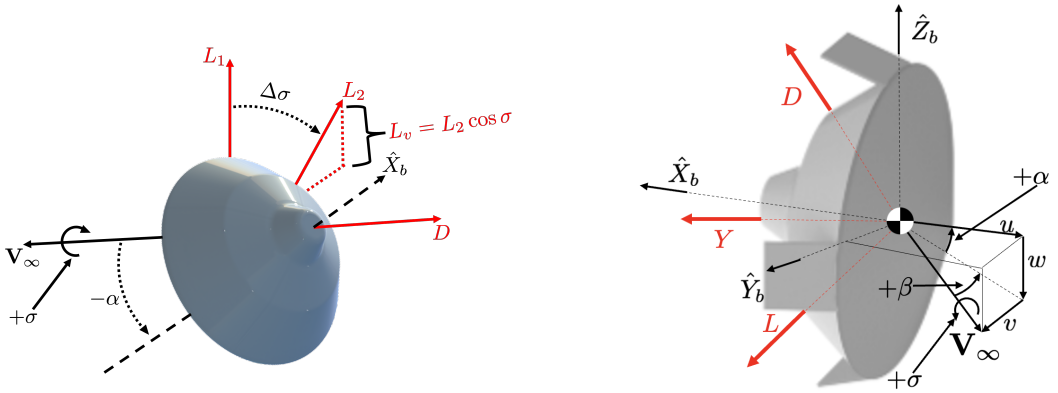

(a) (b)

Figure 1: Aerodynamic angles and forces on blunt-body entry vehicle: (a) bank-angle steering and (b) α-β steering.

Table 1: Vehicle Parameters

Parameter	Value
m	5600 kg
S_{ref}	15.90 m^2
α_{max}	18 deg
β_{max}	18 deg
α_{bank}	-18 deg

Steering Command Generation

To simulate entry performance with active steering, either through the bank angle or a combination of the angle of attack and sideslip angle, steering commands must be generated. In this study, the solutions of optimal control problems are used as a guidance scheme/to provide steering commands to be executed by the vehicle. Using onboard optimal control for generating steering commands allows for the utilization of commands which optimize a number of objectives or constraints. Optimal control also provides solutions which consider the coupled longitudinal and lateral motion. This alleviates the need for open-loop reversals used in current state-of-the-art guidance schemes, potentially improving performance. Most importantly, optimal control provides the best possible solution for a given cost and constraints. By obtaining this best possible performance for a given steering scheme, avoiding the effects of tuning parameters, structure of the guidance scheme, and additional elements, such as control reversals, one can obtain a more equal comparison between bank-angle steering and α-β steering. In this comparison, each steering option exploits its full capability, as a result of not being as dependent on the guidance design. It should be noted that the purpose of using optimal control for steering command generation in this study is to provide a more equal performance comparison and is not to demonstrate real-time optimal control capable of operating on current flight computers.

The optimal control problems used for steering command generation are solved in this study using the General Purpose Optimal Control Software GPOPS-II,[31] a commercial pseudospectral solver. GPOPS-II solves the optimal control problems descried in the next section by using a Legendre-Gauss-Radau quadrature orthogonal collocation method to turn optimal control problems into a finite-dimensional nonlinear programming problem. A diagram showing how the steering command generation interfaces with numerical simulations is shown in Figure 2. Beginning with some initial conditions, the current state and steering commands are passed into the steering command generation at a rate of 0.1 Hz. Using a nominal model for the translational motion, GPOPS-II solves the optimal control problem from the current point in flight out to a terminal descent initiation (TDI) point (planet-relative velocity of 540 m/s[32]), where the vehicle transitions from a high-speed gliding flight to a descent under a parachute or supersonic retropropulsion. The nominal model used for solving the optimal control problems is similar to the nominal model used for the truth dynamics, although there are some simplifying assumptions to ease solutions of the optimal control problems. The dynamics used in the optimal control problems assume Mars is spherical and non-rotating ($\Omega = 0$ rad/s, $J_2 = 0$), the atmosphere is assumed to be exponential, and a fit to the MSL aerodynamics is utilized. This fit is quadratic for C_D and is linear for C_L and C_Y, and the coefficients for these fits are provided in Table 2. Environmental parameters used for the simplified dynamics in GPOPS-II are shown in Table 3.

$$C_D = C_{D,0} + C_{D,\alpha}\alpha^2 + C_{D,\beta}\beta^2 \tag{12}$$

$$C_L = C_{L,\alpha}\alpha \tag{13}$$

$$C_Y = C_{Y,\beta}\beta \tag{14}$$

Once an optimal control program has been solved, there is a full command profile solution for either the bank angle or combination of α and β from the current point out to TDI. The first ten seconds of the command profile is then truncated and commanded to the vehicle. The truth dynamics are then evaluated while executing these commands. The truth dynamics may include dispersions (discussed more in Results section), leading to the truth dynamics deviating further from

Table 2: Parameters for Fitted Aerodynamic Models

Parameter	Value
$C_{D,0}$	1.67
$C_{D,\alpha}$	-2.86/rad^2
$C_{D,\beta}$	-2.86/rad^2
$C_{L,\alpha}$	-1.31/rad
$C_{Y,\beta}$	1.29/rad

Table 3: Environmental Parameters

Parameter	Value
Surface Density	0.012 kg/m^3
Atmospheric Scale Height	11.888 km
Surface Gravity	3.71 m/s^2
Mars Equatorial Radius	3396.20 km

the nominal model used within GPOPS-II. This process of solving optimal control problems and using the first portion of the commands continues until the vehicle reaches TDI. Perfect navigation is assumed when passing the current state into the optimal control solver. Additionally first-order fading-memory filters are used to update the dynamics used within the optimal control solutions to correct for dispersions. For example, the ratio Q_L of the measured lift acceleration (assumed to be a perfect measurement) to the lift calculated by the optimal control dynamics (L_{nom}) is used to compute a corrective factor for the lift for the n^{th} call to the steering commands.

$$Q_L^* = L/L_{nom} \tag{15}$$

$$Q_L(n+1) = Q_L(n) + (1-k)(Q_L^* - Q_L(n)) \tag{16}$$

Here k is a gain used to determine the relative weight of past and current measurements. In this

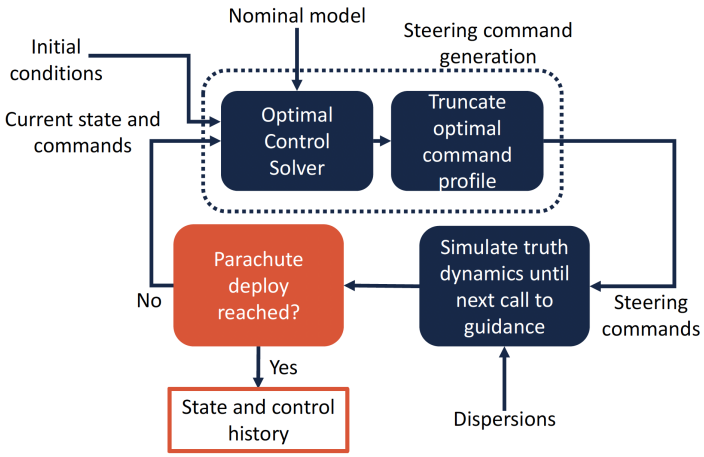

Figure 2: Diagram of steering command generation.

work, it was found that $k = 1$ provided adequate performance. Similar filters can also be computed for the drag and side force.

Optimal Control Problems

Two different optimal control problems are considered in this study. Problem 1 is a maximum altitude problem, which seeks to maximize the entry vehicle altitude $z = r - R_m$ at TDI for increased margin in the descent timeline and landings at higher altitudes, while also reaching a desired longitude and latitude at TDI. Here, θ_{error} and ϕ_{error} correspond to the errors between the actual and desired longitude and latitude, respectively, at TDI. w_1 is a weight to determine how much to emphasize the terminal altitude, $\dot{\mathbf{x}} = \mathbf{f}(\mathbf{x}, \mathbf{u})$ are the simplified dynamics used within the optimal control problem solution, and $V(t_f) = V_f$ is the TDI velocity constraint. There are several constraints for the vehicle using α-β steering to ensure it does not exceed its allocated control authority or obtain an unfair advantage over bank-angle steering. There are constraints on α and β which bound $-\alpha_{max} \leq \alpha \leq \alpha_{max}$ and $-\beta_{max} \leq \beta \leq \beta_{max}$. With these constraints, it is possible that the α-β steering vehicle can have a larger total angle of attack $\alpha_{total} = \cos^{-1}(\cos\alpha \cos\beta)$ than α_{bank} on the bank-angle steering system. This would potentially provide the α-β steering system a larger control authority and would make an unequal comparison between these two steering options. Hence, a path constraint on α_{total} is also included here for α-β steering systems: $\alpha_{total} \leq |\alpha_{bank}|$. To provide realistic vehicle behavior, in which both steering options have finite rate and acceleration limits, the bank angle or angle of attack and sideslip angle, as well as their rates, are recast as elements of the state. The bank acceleration or angle of attack and sideslip accelerations are then used as the control. These rate and acceleration limits are also incorporated as constraints and are those provided in Table 4, unless specified otherwise. After making these changes in the states and control, the state and control vectors are shown in (17) and (18).

$$\mathbf{x}_\sigma = \begin{bmatrix} r & \theta & \phi & V & \gamma & \psi & \sigma & \dot{\sigma} \end{bmatrix}^T \quad \mathbf{x}_{\alpha\text{-}\beta} = \begin{bmatrix} r & \theta & \phi & V & \gamma & \psi & \alpha & \beta & \dot{\alpha} & \dot{\beta} \end{bmatrix}^T \tag{17}$$

$$u_\sigma = \ddot{\sigma} \quad \mathbf{u}_{\alpha\text{-}\beta} = \begin{bmatrix} \ddot{\alpha} & \ddot{\beta} \end{bmatrix}^T \tag{18}$$

Problem 1: Maximum Altitude

$$\begin{aligned}
\min_{\mathbf{u}} \quad & J = -w_1 \frac{z(t_f)}{R_m} + \theta_{error}^2 + \phi_{error}^2 \\
\text{s.t.} \quad & \dot{\mathbf{x}} = \mathbf{f}(\mathbf{x}, \mathbf{u}) \\
& V(t_f) = V_f \\
\alpha\text{-}\beta : \; & \alpha \leq \alpha_{max} \quad -\alpha \leq \alpha_{max} \\
& \beta \leq \beta_{max} \quad -\beta \leq \beta_{max} \\
& \alpha_{total} \leq |\alpha_{bank}| \\
& \dot{\alpha} \leq \dot{\alpha}_{max} \quad -\dot{\alpha} \leq \dot{\alpha}_{max} \\
& \ddot{\alpha} \leq \ddot{\alpha}_{max} \quad -\ddot{\alpha} \leq \ddot{\alpha}_{max} \\
& \dot{\beta} \leq \dot{\beta}_{max} \quad -\dot{\beta} \leq \dot{\beta}_{max} \\
& \ddot{\beta} \leq \ddot{\beta}_{max} \quad -\ddot{\beta} \leq \ddot{\beta}_{max} \\
\sigma : \; & \dot{\sigma} \leq \dot{\sigma}_{max} \quad -\dot{\sigma} \leq \dot{\sigma}_{max} \\
& \ddot{\sigma} \leq \ddot{\sigma}_{max} \quad -\ddot{\sigma} \leq \ddot{\sigma}_{max}
\end{aligned} \tag{19}$$

Table 4: Rate and Acceleration Limits

Parameter	Value
$\dot{\alpha}_{max}$	20 deg/s
$\dot{\beta}_{max}$	20 deg/s
$\ddot{\alpha}_{max}$	5 deg/s^2
$\ddot{\beta}_{max}$	5 deg/s^2
$\dot{\sigma}_{max}$	20 deg/s
$\ddot{\sigma}_{max}$	5 deg/s^2

Problem 2 is the minimum control effort problem. Here the vehicle tries to balance minimizing the effort to control the vehicle while also hitting a desired Cartesian target above the surface of Mars. A given radial distance, longitude, and latitude can be converted to a Cartesian position $(\mathcal{X}, \mathcal{Y}, \mathcal{Z})$ using Equations (20)-(22). The subscript e denotes the error in the Cartesian position, calculated using the difference between the actual and desired position for each of the three coordinates.

$$\mathcal{X} = r\cos\theta\cos\phi \tag{20}$$

$$\mathcal{Y} = r\sin\theta\cos\phi \tag{21}$$

$$\mathcal{Z} = r\sin\phi \tag{22}$$

The control effort can be parameterized by integrating the square of either the bank rate or the α and β rates over the trajectory. Minimizing these integrals results in command profiles in which the vehicle rates are typically small, minimizing the movement or effort by the vehicle. Minimizing control effort with this definition has the potential to decrease propellant and power usage, as well as control system mass. For bank-angle steering the integrand L is

$$L = \dot{\sigma}^2 \tag{23}$$

And for α-β steering this integrand is

$$L = \dot{\alpha}^2 + \dot{\beta}^2 \tag{24}$$

Problem 2: Minimum Control Effort

$$\begin{aligned}
\min_{\mathbf{u}} \quad & J = \int_{t_0}^{t_f} L dt + w_2\left(\mathcal{X}_e^2 + \mathcal{Y}_e^2 + \mathcal{Z}_e^2\right) \\
\text{s.t.} \quad & \dot{\mathbf{x}} = \mathbf{f}(\mathbf{x}, \mathbf{u}) \\
& V(t_f) = V_f \\
\alpha\text{-}\beta : \; & \alpha \leq \alpha_{max} \quad -\alpha \leq \alpha_{max} \\
& \beta \leq \beta_{max} \quad -\beta \leq \beta_{max} \\
& \alpha_{total} \leq |\alpha_{bank}| \\
& \dot{\alpha} \leq \dot{\alpha}_{max} \quad -\dot{\alpha} \leq \dot{\alpha}_{max} \\
& \ddot{\alpha} \leq \ddot{\alpha}_{max} \quad -\ddot{\alpha} \leq \ddot{\alpha}_{max} \\
& \dot{\beta} \leq \dot{\beta}_{max} \quad -\dot{\beta} \leq \dot{\beta}_{max} \\
& \ddot{\beta} \leq \ddot{\beta}_{max} \quad -\ddot{\beta} \leq \ddot{\beta}_{max} \\
\sigma : \; & \dot{\sigma} \leq \dot{\sigma}_{max} \quad -\dot{\sigma} \leq \dot{\sigma}_{max} \\
& \ddot{\sigma} \leq \ddot{\sigma}_{max} \quad -\ddot{\sigma} \leq \ddot{\sigma}_{max}
\end{aligned} \tag{25}$$

Here, w_2 is a weight which can be set to determine how much to emphasize targeting of the desired Cartesian position.

RESULTS

The nominal initial conditions in Table 5 are used for both nominal and dispersed cases, simulated for both steering options and cost functions; these initial conditions are approximately those of current state-of-the-art Mars entry missions. The desired longitude and latitude for both the maximum altitude and minimum effort problems in this study are 12 and 0 deg, respectively. While there is no target altitude for the maximum altitude problem, the minimum effort problem here tries to hit a terminal altitude of 7 km above the equatorial radius of Mars.

Nominal Performance

Nominal trajectory results for both the maximum altitude and minimum control effort problems are provided in Figure 3 for bank-angle steering and α-β steering. On the altitude versus velocity plot in Figure 3a, there are two families of trajectories: one for each of the two optimal control problems considered for steering command generation. For a given objective function the altitude versus velocity curves are similar for bank-angle steering and α-β steering. The latitude and azimuth, though, tend to deviate less from 0 deg and 90 deg, respectively, for the vehicle using α-β steering; this is especially evident for the minimum effort problem. These differences for these two hypersonic steering schemes are a result of the lower coupling over the longitudinal and lateral motion on a vehicle using α-β steering than for a vehicle using bank-angle steering. An α-β steering vehicle can mostly use α and β to control the longitudinal and lateral motion, respectively, whereas a bank-angle steering vehicle must simultaneously use the bank angle to manage both motions, resulting in a deviation in one channel in favor of correcting the other.

Table 5: Nominal Initial Conditions

Parameter	Value
z	135 km
θ	0 deg
ϕ	0 deg
V	6.1 km/s
γ	-15.5 deg
ψ	90 deg
α	0 deg
β	0 deg
$\dot{\alpha}$	0 deg/s
$\dot{\beta}$	0 deg/s

Numerical results for the the vehicle targeting at TDI in these nominal cases are provided in Table 6. Results are included for the baseline 20 deg/s cases shown in Figure 3, as well as alternative 5 deg/s and 1 deg/s cases. Comparing the longitude errors (the columns indicated by θ), the longitude targeting is similar for both steering options across all the rates. These longitude errors translate to downrange errors on the order of hundreds of meters to a few kilometers. Sometimes α-β has an advantage over bank and vice-versa. Comparing the latitude errors (the columns indicated by ϕ)

indicates improved performance of α-β steering over bank-angle steering for both objectives. At 20 deg/s, the latitude errors for α-β steering are half of that of bank-angle steering (several kilometers of crossrange error) for the maximum altitude problem; the latitude errors for the minimum effort problem are on the order of a kilometer and several meters for bank-angle steering and α-β steering respectively. As the allowable rates are decreased, the latitude targeting of α-β steering remains relatively constant, but the errors for latitude targeting increase significantly. For 1 deg/s, the crossrange error for bank-angle steering is on the order of 50 km for both maximum altitude and minimum control effort. At 20 deg/s α-β steering has about a 0.2 km altitude advantage over bank-angle steering (max altitude), and both vehicles have similar targeting capabilities of the 7 km desired altitude (min effort) (the columns indicated by z show the value of the altitude at TDI). As the allowable rates are decreased, both steering options experience drops for the maximum altitude problem. At 1 deg/s, however, α-β steering has about a 4 km altitude advantage over bank-angle steering. For the minimum control effort problem, α-β steering is able to reach close to the target altitude of 7 km even as the vehicle rates are decreased, whereas bank-angle steering exhibits significant drops in altitude as the vehicle rates are decreased.

Table 6: Nominal Targeting Results

Case	θ: σ (deg)	θ: α-β (deg)	ϕ: σ (deg)	ϕ: α-$\beta(deg)$	z: σ (km)	z: α-β (km)
Alt (20 deg/s)	0.103	0.103	-0.048	0.022	9.603	9.826
Effort (20 deg/s)	0.044	0.017	0.017	-1.220×10^{-4}	6.953	7.030
Alt (5 deg/s)	-0.029	0.080	0.305	0.043	8.851	9.809
Effort (5 deg/s)	0.004	0.016	-0.040	1.396×10^{-4}	3.084	7.066
Alt (1 deg/s)	-0.089	-0.047	0.958	0.012	5.015	9.055
Effort (1 deg/s)	-0.068	0.018	0.852	-2.814×10^{-4}	-7.768	7.276

The command profiles flown for these nominal results (20 deg/s) are shown in Figure 4. For the maximum altitude problem, the angle of attack profile has roughly a lift-up lift-down lift-up profile in order to maximize the altitude at TDI while also flying to the desired longitude. There is also a reduction in the angle of attack magnitude near TDI, which increases drag on the vehicle, decelerating it more quickly and preventing losses in altitude. The switches between lift-up and lift-down are similar to those typically seen for maximizing altitude,[33] and there are large increases in the sideslip angle magnitude during these switches when the angle of attack magnitude is decreased. The change in sideslip angle is used to keep α_{total} as large as possible, which reduces drag and prevents further losses in the entry vehicle altitude. The bank-angle steering vehicle also has a mostly lift-up lift-down lift-up profile to simultaneously maximize altitude and hit a desired longitude and latitude. When considering the minimum control effort problem, the angle of attack results show a smooth control profile used to fly to the target latitude, longitude, and altitude while keeping vehicle rates low. Although this control profile is typically well below α_{max}, it does saturate for about 50 s, and there is a switch in both α and β near TDI to fine-tune the error. Other than this behavior near TDI, the sideslip angle profile is near-zero to minimize effort and maintain the vehicle at zero latitude. Lastly, the bank profile is fairly smooth and has both mostly lift-up and mostly lift-down segments in order to fly to the desired target with minimum control effort/movement.

These control profiles help explain several of the trends in Table 6. Even at 20 deg/s, the more decoupled nature of α-β steering (with the sideslip angle controlling the lateral error) results in

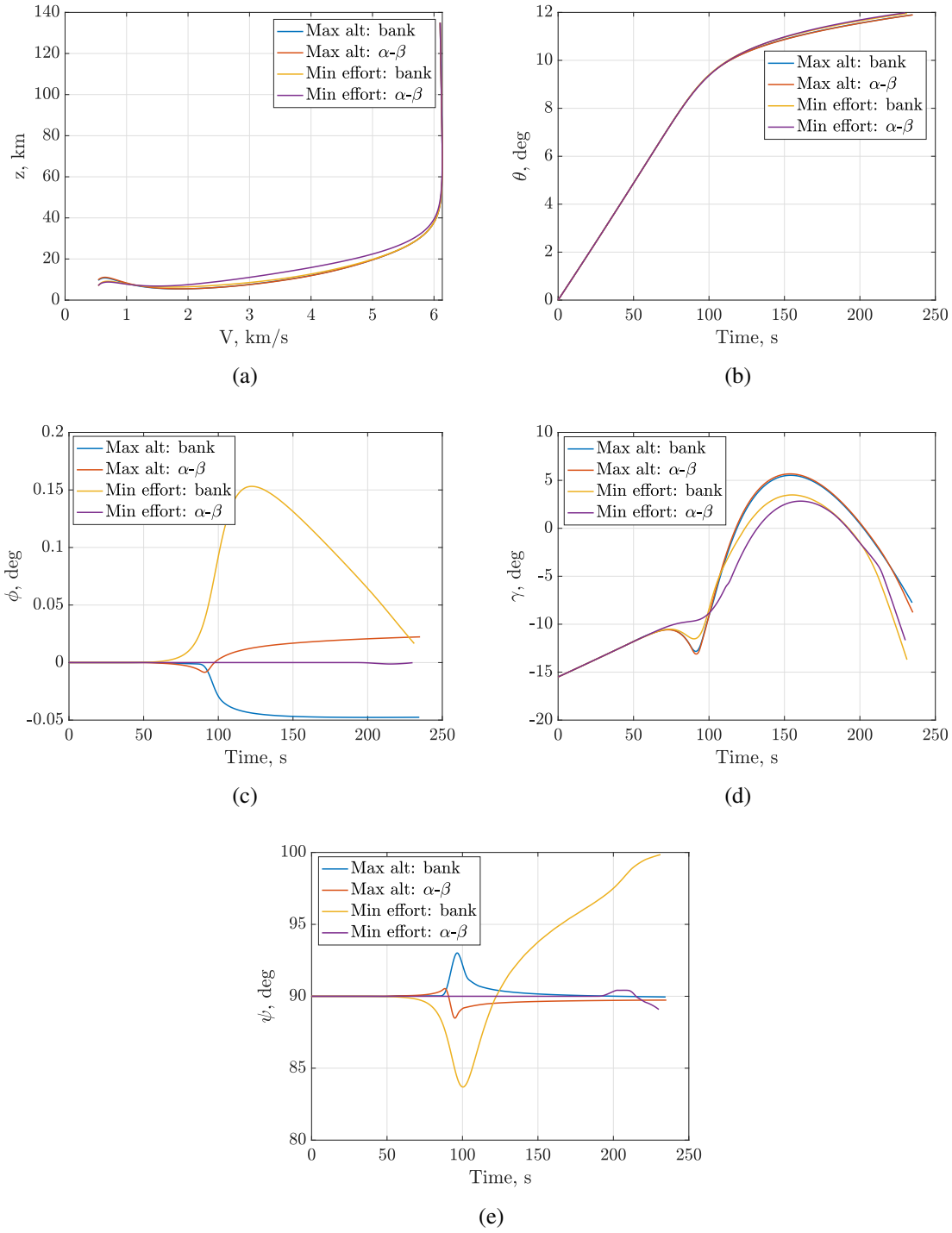

Figure 3: Nominal states for bank-angle steering and α-β steering: (a) altitude versus velocity, (b) longitude, (c) latitude, (d) flight-path angle, and (e) azimuth angle.

a lower lateral error for α-β steering, relative to bank-angle steering. Additionally, the near zero sideslip profile for the minimum effort problem results in a lower latitude error than the maximum altitude sideslip angle profile, which deviates from zero in order reduce drag. The weighting in the objective function may also impact differences in the latitude and longitude targeting between the minimum effort and maximum altitude problems. The differing performance of bank-angle steering and alpha beta steering as vehicle rates are lowered are due to differences in response time. With the same rate of 20 deg/s it takes longer for the bank-angle steering vehicle to maneuver from full lift-up to full-lift down (180 deg maneuver) compared to α-β steering (36 deg maneuver) in the maximum altitude problem. As a result of having a longer maneuvering period between changes in lift, there is a greater amount of time when the vehicle deviates from a theoretically optimal bang-bang profile. This then reduces the altitude maximization performance relative to the α-β steering vehicle. As the allowable rates are decreased for both steering option, this response time difference results in a further deviation in altitude performance between the two steering options. The lower vehicle rates not only impact altitude performance but also latitude performance for bank-angle steering as well. With low rates, such as 1 deg/s, it takes a long time for the bank-angle steering system to null out lateral errors created by the coupled control. With the high degree of coupling on these systems and such low rates, it ends up being challenging to hit a target longitude without having large latitude and altitude errors. The bank profiles also show that no open-loop bank reversals are utilized for steering commands. In fact, the only behavior similar to a bank reversal is are the switches from lift up/lift down, which are done for altitude maximization, not lateral targeting.

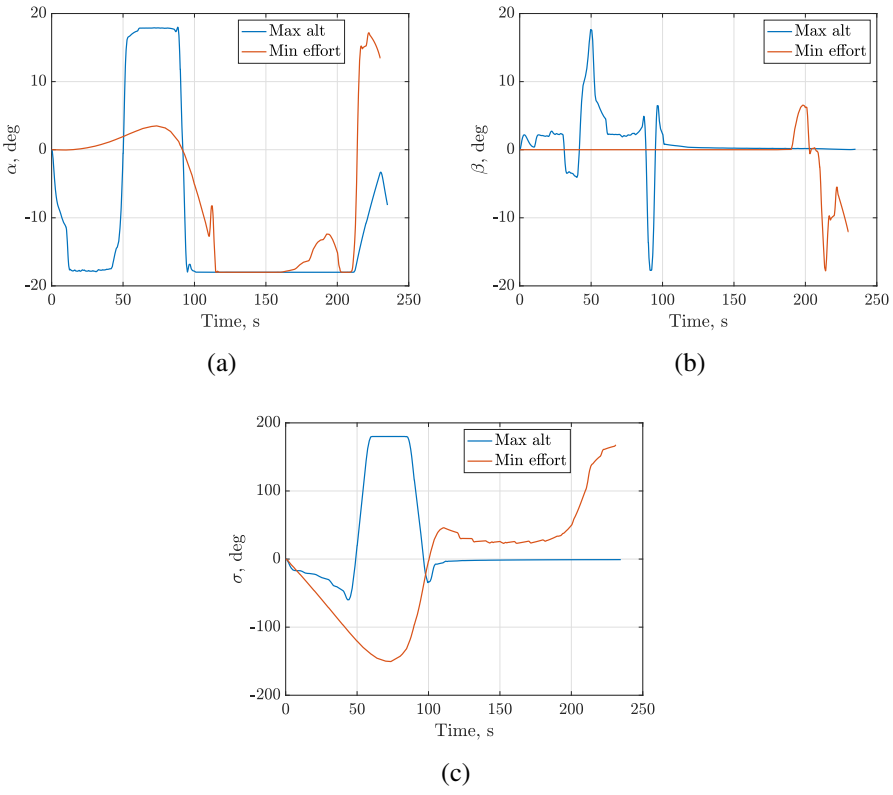

Figure 4: Nominal control profiles for bank-angle steering and α-β steering: (a) angle of attack, (b) sideslip angle, and (c) bank angle.

Dispersed Performance

Uncertainty quantification for both steering schemes was performed using Monte Carlo simulations with 1000 samples; the dispersions used are provided in Table 7. These dispersions include variations in the initial conditions, atmosphere profile, aerodynamic coefficients, and mass, and they allow for a comparison of robustness and targeting between both steering options. Monte Carlo results for the maximum altitude problem with 20 deg/s allowable vehicle rates are shown in Figure 5 and Table 8. Both steering options have a similar mean and standard deviation for the longitude targeting with the corresponding mean downrange errors on the order of several kilometers. Both steering options have a bimodal distribution for the latitude error as a result of the maximum altitude problem tending to bias a single side laterally in a given trajectory. Due to its more decoupled behavior, however, the mean crossrange error for α-β steering is on the order of tens of meters, whereas the bank-angle steering results are on the order of hundreds of meters. Furthermore, the standard deviation is about for α-β steering is about half of that of bank-angle steering. The standard deviation for altitude maximization is slightly higher for α-β steering, but the mean altitude, as well as the altitudes across all percentiles, are about 0.25 to 0.3 km higher for α-β steering, relative to bank-angle steering. This altitude advantage is also evident in Figure 5c, where the α-β histogram is noticeably shifted to the right of the bank-angle steering histogram. While this altitude advantage is only a fraction of a kilometer, all Mars entry missions to date have landed at negative altitudes (e.g. -1.3 km and -2.56 km for the Mars Exploration Rovers[34] and Mars 2020,[35] respectively). Therefore, even a small altitude advantage may be helpful for either landing at new destinations or for adding margin in the descent timeline. Hence, at 20 deg/s of rotational rates, both vehicles have similar targeting and robustness for the longitude, α-β steering has improved targeting and robustness for the latitude, and α-β steering has improved altitude maximization capabilities (although the variation of altitude maximization is similar for both steering options).

Table 7: Monte Carlo Dispersions

Variable	Dispersion	Distribution
Initial altitude	± 2.8 km 3σ	Gaussian
Initial longitude	± 0.017 deg 3σ	Gaussian
Initial latitude	± 0.013 deg 3σ	Gaussian
Initial velocity	± 2 m/s 3σ	Gaussian
Initial flight-path angle	± 0.2 deg 3σ	Gaussian
Initial azimuth	± 0.006 deg 3σ	Gaussian
Atmosphere profile	1000 Mars GRAM atmospheres	-
Hypersonic C_A	$\pm 0.03\%$ 3σ	Gaussian
Hypersonic C_N	$\pm 0.05\%$ 3σ	Gaussian
Supersonic C_A	$\pm 0.1\%$ 3σ	Gaussian
Supersonic C_N	$\pm 0.08\%$ 3σ	Gaussian
Mass	± 2 kg 3σ	Gaussian

Monte Carlo results for maximizing altitude with lower rates of 5 deg/s and 1 deg/s are provided in Tables 9 and 10, respectively. Similar to the nominal cases, as the allowable rates are lowered, the mean terminal altitude performance decreases. When decreasing to 5 deg/s, there is only a small drop in altitude performance for α-β steering, but bank-angle steering experiences a larger

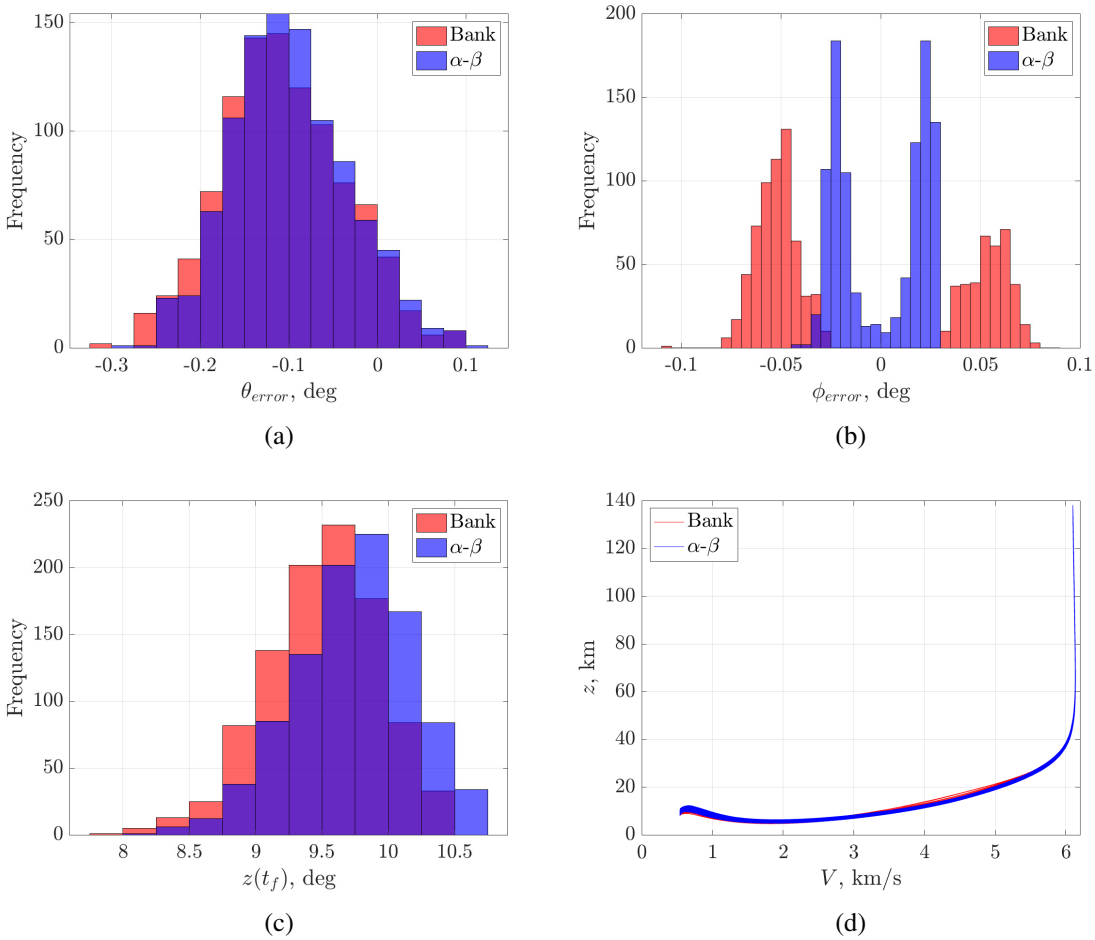

Figure 5: Monte Carlo results for maximizing altitude: (a) histogram of longitude results, (b) histogram of latitude results, (c) histogram of altitude results, and (d) altitude versus velocity profiles for all Monte Carlo samples.

Table 8: Maximum Altitude Results (20 deg/s)

Parameter	θ: σ (deg)	θ: α-β (deg)	ϕ: σ (deg)	ϕ: α-β (deg)	z: σ (km)	z: α-β (km)
Mean	-0.106	-0.097	-0.012	7.260×10^{-4}	9.515	9.751
SD	0.071	0.067	0.053	0.022	0.443	0.462
0.1%	-0.312	-0.280	-0.106	-0.044	7.967	8.069
1%	-0.263	-0.243	-0.073	-0.032	8.375	8.617
10%	-0.193	-0.177	-0.063	-0.026	8.915	9.131
50%	-0.110	-0.103	-0.044	0.009	9.544	9.78
90%	-0.009	-0.005	0.062	0.026	10.052	10.331
99%	0.076	0.077	0.073	0.030	10.486	10.795
99.9%	0.122	0.142	0.092	0.034	10.631	10.960

drop resulting in α-β steering having about a 1 km altitude advantage. Decreasing further to 1 deg/s, α-β steering has over a 4 km altitude advantage over bank-angle steering. Both steering systems all have standard deviations of around 0.5 km across all rates, so changing the rate and steering system essentially represents a horizontal shift in the distribution. The latitude targeting for α-β steering remains relatively constant, with mean errors on the order of hundreds of meters at the worst and standard deviations on the order of hundreds of meters to a few kilometers, as the vehicle rates are decreased. For bank-angle steering, however, these latitude errors have means and standard deviations on the order of 50 km and 10 km, respectively. As was for the nominal cases, the lower response time (i.e. longer time to maneuver due to larger angles to rotate through) and coupled motion over the longitudinal and lateral channels on bank-angle steering vehicles results in a much more significant reduction in the altitude maximization performance and lateral targeting and robustness, relative to the α-β steering system. While there is some variation in the longitude targeting as the rates are decreased, the mean and standard deviation are the same order of magnitude across both steering schemes and rates.

Table 9: Maximum Altitude Results (5 deg/s)

Parameter	θ: σ (deg)	θ: α-β (deg)	ϕ: σ (deg)	ϕ: α-β (deg)	z: σ (km)	z: α-β (km)
Mean	0.027	-0.076	0.277	0.011	8.799	9.726
SD	0.069	0.067	0.136	0.042	0.462	0.469
0.1%	-0.197	-0.272	-0.312	-0.058	7.241	8.015
1%	-0.131	-0.224	-0.301	-0.053	7.639	8.573
10%	-0.057	-0.159	0.282	-0.047	8.174	9.083
50%	0.024	-0.082	0.306	0.038	8.822	9.752
90%	0.117	0.012	0.331	0.048	9.366	10.308
99%	0.195	0.089	0.356	0.055	9.859	10.789
99.9%	0.236	0.150	0.362	0.060	10.052	10.915

Table 10: Maximum Altitude Results (1 deg/s)

Parameter	θ: σ (deg)	θ: α-β (deg)	ϕ: σ (deg)	ϕ: α-β (deg)	z: σ (km)	z: α-β (km)
Mean	0.058	0.049	0.920	0.002	4.723	8.996
SD	0.097	0.069	0.246	0.012	0.516	0.506
0.1%	-0.284	-0.182	-0.981	-0.021	2.880	7.252
1%	-0.159	-0.104	-0.946	-0.017	3.197	7.789
10%	-0.077	-0.037	0.932	-0.013	4.058	8.333
50%	0.070	0.046	0.952	0.009	4.786	9.024
90%	0.178	0.141	0.972	0.014	5.303	9.636
99%	0.243	0.221	0.989	0.021	5.797	10.121
99.9%	0.296	0.279	1.003	0.024	6.068	10.363

Monte Carlo results for the minimum effort problem, targeting an altitude of 7 km, are provided in Figure 6 and Table 11. These results show both steering schemes are able to provide similar longitude and altitude targeting/robustness. In particular, the mean longitudes are about twice as large for bank-angle steering as they are for α-β steering (order of several kilometers), and the

standard deviations are similar. The mean altitude targeting between the two vehicle options is slightly better for bank-angle steering, but the standard deviation is slightly smaller (difference for both is on the order of tens to hundreds of meters). There is, however, a noticeable difference in latitude targeting between the two steering options. The vehicle using α-β has means and standard deviations for crossrange error on the order tens of meters, whereas the vehicle using bank-angle steering has crossrange error mean and standard deviations on the order of hundreds of meters to several kilometers. The larger crossrange error associated with bank-angle steering is again a result of the high coupling over the longitudinal and lateral motion. As shown in Figure 3c, the bank angle results in a deviation from zero latitude for longitude/altitude targeting and then tries to come back as close to zero as possible at TDI. With some dispersions, the vehicle is unable to null out this latitude error as much without sacrificing performance in longitude/altitude, leading to larger latitude errors. α-β steering does not have this issue, as it is significantly more decoupled and can use α mostly for control over the longitude and altitude targeting and β mostly for latitude targeting.

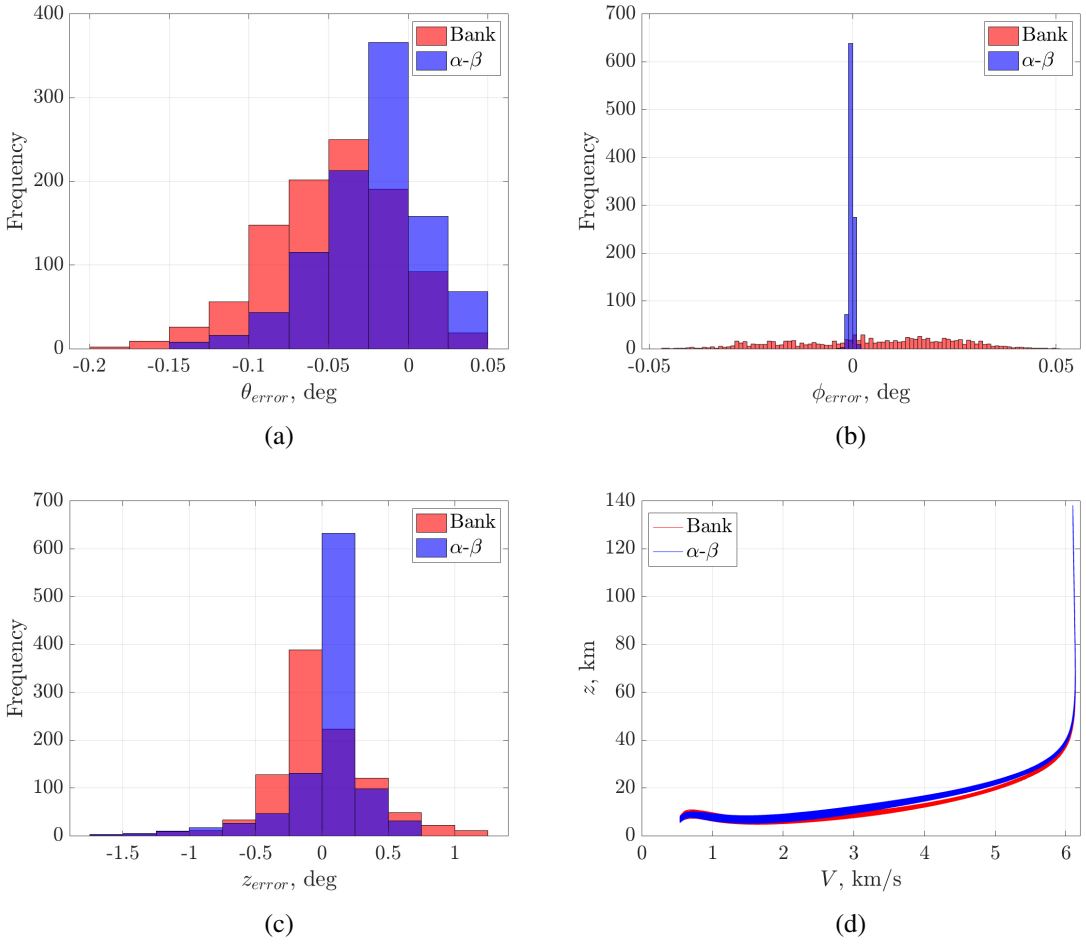

Figure 6: Monte Carlo results for minmizing control effort: (a) histogram of longitude results, (b) histogram of latitude results, (c) histogram of altitude results, and (d) altitude versus velocity profiles for all Monte Carlo samples.

The total angle of attack used during entry can be illustrative of the control authority used during

Table 11: Minimum Control Effort Results (7 km Altitude Target)

Parameter	θ: σ (deg)	θ: α-β (deg)	ϕ: σ (deg)	ϕ: α-β (deg)	z: σ (km)	z: α-β (km)
Mean	-0.047	-0.020	0.005	2.990×10^{-4}	6.989	7.032
SD	0.040	0.034	0.020	5.150×10^{-4}	0.366	0.304
0.1%	-0.182	-0.147	-0.046	-0.004	5.442	5.337
1%	-0.152	-0.119	-0.039	-0.001	5.869	5.786
10%	-0.099	-0.063	-0.024	-9.370×10^{-4}	6.648	6.727
50%	-0.045	-0.017	0.006	-1.910×10^{-4}	6.938	7.068
90%	0.003	0.022	0.029	1.280×10^{-4}	7.454	7.294
99%	0.044	0.055	0.042	0.001	8.010	7.664
99.9%	0.064	0.073	0.052	0.004	8.250	7.843

entry; a lower total angle of attack usage could have benefits such as lower heating on the leeward side of the entry (particularly useful for deployable or inflatable heatshields with open back shell designs) as well as a lower control system mass (e.g. smaller flap system needed). For a given Monte Carlo simulation, the percent of cases which have a saturated α_{total}, as well as the mean α_{total} used across all Monte Carlo samples, can be computed. The results in Figure 7 show these data for Monte Carlo simulations with several desired terminal altitudes. As the desired terminal altitude is decreased, the entry vehicle does not need as much lift to loft itself and can fly with a lower α_{total}. Hence, there is a reduction in both the mean α_{total} as well as the percentage of cases in which α_{total} saturates. One previous study of α-β steering found that a vehicle using α-β steering may be able to obtain improved targeting performance over a bank-angle steering vehicle while also using a significantly lower α_{total}.[22] Monte Carlo analysis with 16 deg and 14 deg limits on α_{total} and α_{bank} were carried out, and results are provided in Tables 12 and 13, respectively. These results indicate that successful performance may be possible with lower angle of attack values on both steering options, although the mean and standard deviation for altitude performance degrades as the α_{total} limit is decreased. Comparing the reduction in altitude performance between the two steering options, the mean altitude for bank-angle steering tends to degrade more significantly than alpha-beta steering, although both have the same order of magnitude. While the altitude targeting performance decreases due to insufficient lift to loft the altitude, the latitude and longitude targeting and robustness tends to stay similar of even improve in some cases—particularly with $\alpha_{total,max} = 14$ deg. With insufficient lift to hit the target altitude, the vehicles instead spends their control authority to more accurately reach the target latitude and longitude. Hence, it is possible for successful latitude/longitude at lower total angles of attack, but altitude targeting may be compromised. Although the performance for alpha-beta steering is better than bank-angle steering across longitude, latitude, and altitude for all of the reduced control authority cases, the performance differences are small and do not indicate a significantly lower α_{total} can be used on alpha-beta steering, relative to bank-angle steering. Larger differences may occur for steering commands consisting of bank reversals.

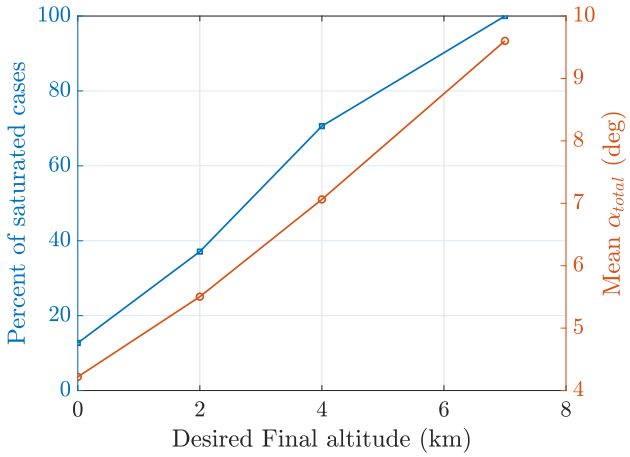

Figure 7: Total angle of attack usage during entry.

Table 12: Minimum Control Effort Results ($\alpha_{total,max} = 16$ deg)

Parameter	θ: σ (deg)	θ: α-β (deg)	ϕ: σ (deg)	ϕ: α-β (deg)	z: σ (km)	z: α-β (km)
Mean	-0.029	-0.009	3.860×10^{-4}	-3.970×10^{-4}	7.188	7.010
SD	0.038	0.031	0.003	8.160×10^{-4}	0.452	0.433

Table 13: Minimum Control Effort Results ($\alpha_{total,max} = 14$ deg)

Parameter	θ: σ (deg)	θ: α-β (deg)	ϕ: σ (deg)	ϕ: α-β (deg)	z: σ (km)	z: α-β (km)
Mean	-0.002	0.008	-3.300×10^{-5}	9.800×10^{-5}	6.396	6.560
SD	0.036	0.026	9.170×10^{-4}	3.100×10^{-4}	0.636	0.698

CONCLUSIONS

This study uses a pseudospectral optimal control solver to generate steering commands for vehicles using either bank-angle steering or alpha-beta steering during a Mars entry, where optimal control problems are solved many times over a single trajectory. Both maximum altitude and minimum control effort objectives are considered within the optimal control problems, and nominal and dispersed cases are assessed for a future large Mars entry vehicle. By using optimal control for steering commands, the bank-angle steering vehicle uses a command profile considering both the longitudinal and lateral motion, alleviating the need for open-loop bank reversals. This elimination of bank reversals and user specified design and tuning helps to provide a more equal comparison of bank-angle steering and alpha-beta steering. Results indicate both steering options provide similar longitude targeting. Alpha-beta steering is shown to provide significantly improved latitude targeting and robustness, especially for the minimum effort problem, as a result of the more decoupled nature of this hypersonic steering scheme. Alpha-beta steering also has both an altitude targeting and altitude maximization advantage, relative to bank-angle steering. At 20 deg/s, the vehicle using alpha-beta steering has about a 0.25 km altitude advantage over bank-angle steering. As the allow-

able vehicle rates are lowered, this altitude advantage as well as the latitude error of the bank-angle steering vehicle grow significantly.

ACKNOWLEDGEMENTS

This work was supported by a NASA Space Technology Graduate Research Opportunity.

REFERENCES

[1] D. W. Way, S. Dutta, C. Zumwalt, and D. Blette, "Assessment of the Mars 2020 Entry, Descent, and Landing Simulation," *AIAA SciTech Forum*, American Institute of Aeronautics and Astronautics Inc., 2022, 10.2514/6.2022-0421.

[2] G. F. Mendeck and L. C. McGrew, "Entry Guidance Design and Postflight Performance for 2011 Mars Science Laboratory Mission," *Journal of Spacecraft and Rockets*, Vol. 51, No. 4, 2014, 10.2514/1.A32737.

[3] C. A. Graves and J. C. Harpold, "Apollo Experience Report: Mission Planning for Apollo Reentry," Tech. Rep. NASA-TN-D-6725, NASA Manned Spacecraft Center, 1972.

[4] J. C. Harpold and C. A. Graves, "Shuttle Entry Guidance," Tech. Rep. NASA-TM-D-79949, NASA Johnson Space Center, 1979.

[5] S. H. Bairstow and G. H. Barton, "Orion Reentry Guidance With Extended Range Capability Using PredGuid," *AIAA Guidance, Navigation, and Control Conference*, American Institute of Aeronautics and Astronautics Inc., 2007, 10.2514/6.2007-6427.

[6] A. D. Cianciolo, R. A. Lugo, A. M. Korzun, A. C. Adam C. Slagle, E. M. Queen, R. A. Dillman, and R. W. Powell, "Low Lift-to-Drag Morphing Shape Design," *AIAA SciTech Forum*, American Institute of Aeronautics and Astronautics Inc., 2020, 10.2514/6.2020-1266.

[7] P. Lu, C. J. Cerimele, M. A. Tigges, and D. A. Matz, "Optimal Aerocapture Guidance," *Journal of Guidance, Control, and Dynamics*, Vol. 38, No. 4, 2015, pp. 553–565, 10.2514/1.G000713.

[8] P. Lu, "Entry guidance: A unified Method," *Journal of Guidance, Control, and Dynamics*, Vol. 37, 2014, pp. 713–728, 10.2514/1.62605.

[9] A. M. Korzun, K. J. Murphy, and K. T. Edquist, "Supersonic Aerodynamic Characteristics of Blunt Body Trim Tab Configurations," *Fluid Dynamics and Co-located Conferences*, American Institute of Aeronautics and Astronautics Inc., 2013, 10.2514/6.2013-2809.

[10] A. D. Steltzner, M. A. San Martin, T. P. Rivellini, A. Chen, and D. Kipp, "Mars Science Laboratory Entry, Descent, and Landing System Development Challenges," *Journal of Spacecraft and Rockets*, Vol. 51, No. 4, 2014, 10.2514/1.A32866.

[11] A. A. Dyakonov, M. Schoenenberger, W. I. Scallion, J. W. Van Norman, L. A. Novak, and C. Y. Tang, "Aerodynamic Interference Due to MSL Reaction Control System," *41st AIAA Thermophysics Conference*, American Institute of Aeronautics and Astronautics Inc., 2009, 10.2514/6.2009-3915.

[12] M. Schoenenberger, J. Van Norman, M. Rhode, and J. Paulson, "Characterization of Aerodynamic Interactions with the Mars Science Laboratory Reaction Control System Using Computation and Experiment," *51st AIAA Aerospace Sciences Meeting*, American Institute of Aeronautics and Astronautics Inc., 2013, 10.2514/6.2013-971.

[13] A. A. Dyakonov, C. E. Glass, P. N. Desai, and J. W. Van Norman, "Analysis of Effectiveness of Phoenix Entry Reaction Control System," *Journal of Spacecraft and Rockets*, Vol. 48, No. 5, 2011, 10.2514/1.40965.

[14] R. A. Lugo, S. Dutta, D. Matz, B. J. Johnson, A. R. Pensado, E. Roelke, J. T. Aguirre, and R. Powell, "Performance Analysis of SmallSat Aerocapture at Venus," *AIAA SCITECH 2023 Forum*, American Institute of Aeronautics and Astronautics Inc., 2023, 10.2514/6.2023-0878.

[15] B. Margolis, W. Okolo, S. N. D'Souza, and B. J. Johnson, "Pterodactyl: Guidance and Control of a Symmetric Deployable Entry Vehicle using an Aerodynamic Control System," *AIAA Scitech 2021 Forum*, 2021, 10.2514/6.2021-0764.

[16] R. A. Lugo, R. W. Powell, and A. D. Cianciolo, "Overview of a Generalized Numerical Predictor-Corrector Targeting Guidance with Application to Human-Scale Mars Entry, Descent, and Landing," *AIAA SciTech Forum*, American Institute of Aeronautics and Astronautics Inc., 2020, 10.2514/6.2020-0846.

[17] R. Deshmukh, *System Analysis of a Numerical Predictor-Corrector Aerocapture Guidance Architecture*. PhD thesis, Purdue University, 2021.

[18] D. Engel and Z. R. Putnam, "Control of a Blunt Body Mars Entry Vehicle with Flaps Using Model Predictive Control," *AIAA SCITECH 2022 Forum*, American Institute of Aeronautics and Astronautics Inc., 2022, 10.2514/6.2022-1651.

[19] B. M. Atkins and E. M. Queen, "Internal Moving Mass Actuator Control for Mars Entry Guidance," *Journal of Spacecraft and Rockets*, Vol. 52, No. 5, 2015, pp. 1294–1310, 10.2514/1.A32970.

[20] D. A. Matz, C. J. Cerimele, and R. R. Sostaric, "Comparison of Aerocapture Performance Using Bank Control and Direct Force Control with Two Human-Scale Vehicles at Mars," *AIAA SciTech Forum*, American Institute of Aeronautics and Astronautics Inc., 2020, 10.2514/6.2020-1738.

[21] B. J. Johnson, D. Rocca-Bejar, P. Lu, B. E. Nikaido, B. C. Yount, S. N. D'souza, and Z. Hays, "Pterodactyl: The development and performance of guidance algorithms for a mechanically deployed entry vehicle," *AIAA Scitech 2020 Forum*, American Institute of Aeronautics and Astronautics Inc., 2020, 10.2514/6.2020-1011.

[22] A. D. Cianciolo and R. W. Powell, "Entry, Descent, and Landing Guidance and Control Approaches to Satisfy Mars Human Landing Mission Criteria," *Advances in the Astronautical Sciences*, Vol. 160, No. AAS 17-254, 2017.

[23] E. M. Palmer and A. V. Rao, "Mars Entry Optimal Trajectory Generation, Guidance, and Control," *AIAA SciTech 2022 Forum*, American Institute of Aeronautics and Astronautics Inc., 2022, 10.2514/6.2022-2390.

[24] R. T. Bibeau and D. S. Rubenstein, "Trajectory Optimization for a Fixed-Trim Reentry Vehicle using Direct Collocation and Nonlinear Programming," *18th Applied Aerodynamics Conference*, American Institute of Aeronautics and Astronautics Inc., 2000, 10.2514/6.2000-4262.

[25] K. Tracy and Z. Manchester, "CPEG: A Convex Predictor-corrector Entry Guidance Algorithm," *IEEE Aerospace Confrerence*, Institute of Electrical and Electronics Engineers Inc., 2022, 10.1109/AERO53065.2022.9843641.

[26] K. S. Tracy, G. Falcone, and Z. Manchester, "Robust Entry Guidance with Atmospheric Adaptation," *AIAA SCITECH 2023 Forum*, American Institute of Aeronautics and Astronautics Inc., 2023, 10.2514/6.2023-0301.

[27] J. A. Rataczak, J. W. McMahon, and I. D. Boyd, "Predictor-Corrector Aerocapture Guidance using Convex Programming," *International Planetary Probe Workshop*, 2023.

[28] A. A. Dyakonov, M. Schoenenberger, and J. W. Van Norman, "Hypersonic and Supersonic Static Aerodynamics of Mars Science Laboratory Entry Vehicle," *43rd AIAA Thermophysics Conference*, American Institute of Aeronautics and Astronautics Inc., 2012, 10.2514/6.2012-2999.

[29] C. Justus, "A Mars Global Reference Atmospheric Model (MARS-GRAM) for Mission Planning and Analysis," *28th Aerospace Sciences Meeting*, American Institute of Aeronautics and Astronautics Inc., 1990, 10.2514/6.1990-4.

[30] S. Sell, G. Bonfiglio, B. Harper, M. Ivanov, M. Lefland, C. O'Farrell, C. Sackier, and A. Zimmer, "Mars Sample Retrieval Lander Entry Descent and Landing Overview," *International Planetary Probe Workshop*, 2022.

[31] M. A. Patterson and A. V. Rao, "GPOPS-II: A MATLAB Software for Solving Multiple-Phase Optimal Control Problems Using Hp-Adaptive Gaussian Quadrature Collocation Methods and Sparse Nonlinear Programming," *ACM Trans. Math. Softw.*, Vol. 41, No. 1, 2014, 10.1145/2558904.

[32] G. F. Mendeck and L. E. Craig, "Entry Guidance for the 2011 Mars Science Laboratory Mission," *AIAA Atmospheric Flight Mechanics Conference*, American Institute of Aeronautics and Astronautics Inc., 2011, 10.2514/6.2011-6639.

[33] C. G. Lorenz and Z. R. Putnam, "Entry Trajectory Options for High Ballistic Coefficient Vehicles at Mars," *Journal of Spacecraft and Rockets*, Vol. 56, No. 3, 2019, pp. 811–822, 10.2514/1.A34262.

[34] J. K. Erickson, R. Manning, and M. Adler, "Mars Exploration Rover: Launch, Cruise, Entry, Descent, and Landing," *55th International Astronautical Congress of the International Astronautical Federation, the International Academy of Astronautics, and the International Institute of Space Law*, 10.2514/6.IAC-04-Q.3.A.03.

[35] C. D. Karlgaard, M. Schoenenberger, S. Dutta, and D. W. Way, "Mars Entry, Descent, and Landing Instrumentation 2 Trajectory, Aerodynamics, and Atmosphere Reconstruction," *Journal of Spacecraft and Rockets*, Vol. 60, No. 1, 2023, pp. 199–214, 10.2514/1.A35440.